Clays and Clay Minerals, Vol. 44, No. 1, 22–31, 1996.

HEMATITE AND GOETHITE FROM DURICRUSTS DEVELOPED BY LATERITIC CHEMICAL WEATHERING OF PRECAMBRIAN BANDED IRON FORMATIONS, MINAS GERAIS, BRAZIL

E. RAMANAIDOU,[1] D. NAHON,[2] A. DECARREAU,[3] AND A. J. MELFI[4]

[1] CSIRO -Division of Exploration and Mining. Private Bag. P.O. Wembley, W.A. 6014, Australia

[2] Geosciences de l'Environnement URA 132 CNRS, Faculté des Sciences St Jérôme, Université d'Aix-Marseille III Case 431, 13397 Marseille Cedex 20, France

[3] Argiles, Sols, Altérations. URA 721 CNRS,** Université de Poitiers, 40 Av. Recteur Pineau, 86000, Poitiers, France

[4] Departamento de Geofisica/Núcleo de Pesquisa em Geoquímica e Geofisica da Litosfera, Universidade de São Paulo Av. Miguel Stefano 4200, São Paulo, Brazil

Abstract—The upper 15–20 m of a 200 m thick lateritic weathering profile on Precambrian itabirites of Capanema, Brazil, reveals a genetic pathway for the formation of hematitic and goethitic nodules in the ferruginous crust through a very fine grain Al-hematite and Al-goethite mixture, called here the brick-red-material (brm). This evolution develops between the soft saprolite and a 10 m thick indurated ferruginous crust. The soft saprolite retains the original structures of the itabirite and is characterized by almost complete dissolution of quartz, the development of goethite septa, and the partial dissolution of primary hematite. Near the contact with the overlying ferruginous crust, the brm is gradually filling voids as well as replacing primary hematite and goethite in the saprolite. In the upper indurated crust, the brm transforms into coarse structureless ferruginous nodules (aluminous hematites and goethites) and is the precursor of the hematito-goethitic nodules of the crusts. Crystallization of newly-formed Al-goethite and Al-hematite within the brm occurs without detectable amounts of amorphous iron oxides of ferrihydrite precursors.

Key Words—Hematite, Goethite, Laterite, Mössbauer Spectrometry.

INTRODUCTION

The lateritic weathering of iron-bearing "itabirites" or banded iron formations at Capanema mine (Minas Gerais, Brazil) has led to the development of iron ore (Ramanaidou 1989). The iron and silica rich parent rock typically have a marked bedding at a high angle to the ground surface which has allowed deep penetration of weathering fluids particularly in humid tropical climates. Few studies have examined these types of deposits, most of which were restricted to the lower part of the weathering profile (Eichler 1968; Melfi et al. 1976; de Campos 1980, Morris 1983). This study examines the genesis of the ferruginized zone of the 15 to 20 meters upper portion of the weathering profile. Observations similar to those at Capanema were previously made in West Africa (Nahon 1970) and in Brazil (Melfi et al. 1976), but were not subjected to crystallochemical studies as detailed in the present case. These earlier studies are useful to confirm the generalization of the more detailed results presented here. We examined complete weathering profiles exposed in active quarry faces and drill cores at Capanema, in the Quadrilatero Ferrifero of Brazil whose surface of about 7,000 km^2 is located in the center of the state of Minas Gerais, 450 km north of Rio de Janeiro (Dorr 1969). The first part of this paper details the petrology and the physico-chemistry of the upper part of the weathering profile, especially the nature of the Fe oxy-hydroxides. The second part describes processes for the genesis of indurated iron-bearing crust often called "canga."

ANALYTICAL TECHNIQUES

The weathered profiles were sampled during several field studies between 1984 and 1986.

Petrographic studies were completed on polished thin sections. Mineral identifications were based on X-ray diffraction techniques recorded at 1/8° 2 θ/min with Philips PW 1729-1730 diffractometers equipped with a Co tube with Fe filter. Quartz was added as an internal standard. Some X-ray measurements were performed on microsampled powders (handpicked under binoculars) as well as on thin sections using a linear detector (Elphyse) according to the method described by Rassineux et al. (1988). Unit cell parameters of goethite and hematite were computed using the unit cell program proposed by Tournarie (1969) from 020, 110, 120, 130, 021, 040, 111, 121, 140 and 221 (hkl) for peaks for goethite and 021, 104, 110, 113, 024, 116, 214 and 300 peaks for hematite. The mean crystal dimensions (MCD_{hkl}) of hematite and goethite were evaluated from widths at half height after using Warren's correction for instrumental broadening (Klug and

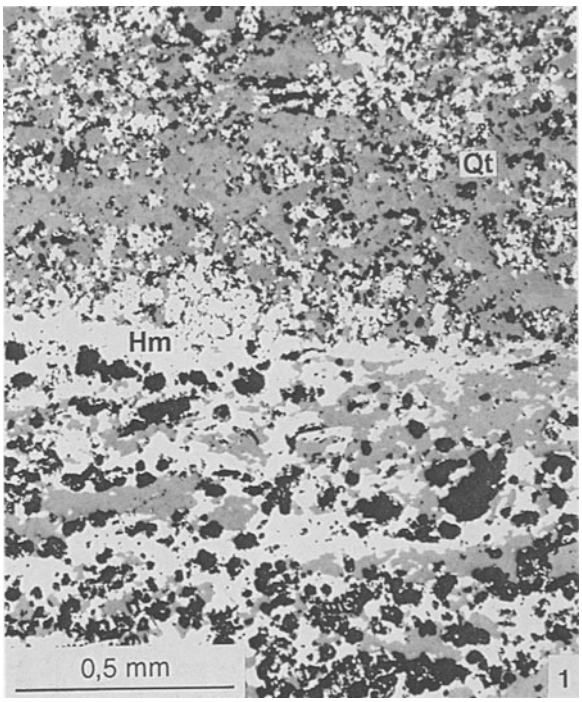

Figure 1. Alternating layers of quartz (Qt) and iron oxides (Hm: hematite). Reflected light.

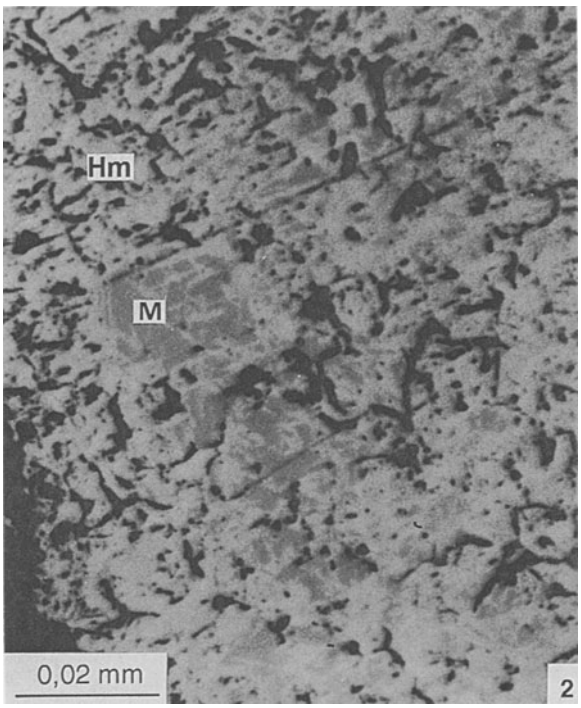

Figure 2. Relict magnetite (M) replaced by hematite (Hm). Reflected light.

Alexander 1962). This approach, rather simple, does not take into account strain broadening (Klug and Alexander 1974) but gives useful relative MCD values.

The quantification of Al substitution in iron oxides can be estimated from unit cell parameters, but is often difficult to estimate because other parameters, like crystallinity, influence the measurements (Schwertmann 1988a). For goethite, Al substitution was estimated from the C parameters using the method of Schulze (1982), because this unit cell parameter is essentially independant of crystallinity. For hematite, numerous data exist showing evolution of unit cell parameters with both Al substitutions, crystallinity, and structural OH (Stanjek and Schwertmann 1992). In the more recent and accurate study of this problem Stanjek and Schwertmann (1992) give multiple regression equations for hematite cell parameters as a function of Al and loss of ignition (LOI). This approach was used in this paper for hematite pure sample. For samples in which hematite is mixed with goethites or other iron hydroxides, the measured LOI cannot be used and the method of Stanjek and Schwertmann cannot operate. Regression functions given by Perinet and Lafont (1972) and Schwertmann and Kampf (1985) can be used for mixed samples. The functions give slightly different Al substitution values but are consistent, showing the same trends (Table 2).

Chemical data were obtained from thin sections with a Camebax electron probe. Bulk density was measured on dried rock samples by weighting and coating them with parafin wax prior to analysis by means of Atomic Absorption Spectroscopy (AA5) with a Perkin Elmer 2380 apparatus after fusion of sample using sodium metaborate.

Organic carbon was measured as CO_2 after firing samples at 1000°C under oxygen atmosphere using a Wösthoff carmograph apparatus.

Mössbauer spectra were recorded in 512 channels of an Elscint AME 30 spectrometer in triangular mode. A ^{57}Co source in a rhodium matrix of nominal strength 25 m Cl was used with NaI scintillator as the γ ray detector. Velocity calibration was made using a high-grade Fe lamina. The Mössbauer spectra were recorded at room temperature and at 77°K. All data were computer-fitted with Lorentian components by a least square program.

STAGES OF WEATHERING

The fresh parent rock observed in cores is a highly indurated and microfolded itabirite with an average schistosity dipping 45–55°. The itabirite consists of alternating from centimeter to micrometer scale microlayers of white quartz (interlocked grains 40 to 60 μm in size with wavy extinction and recrystallization in microfolds) and of black microlayers (Figure 1) consisting of tabular to ellipsoidal grains of hematite (40 to 50 μm in size) with scattered irregularly-shaped grains of partly oxidized magnetite (Figure 2). About

https://doi.org/10.1346/CCMN.1996.0440102 Published online by Cambridge University Press

Table 1. Average chemical composition of minerals of "fresh itabirite" of Capanema.

	Microprobe Analyses										
	SiO_2	Fe_2O_3	Al_2O_3	MgO	MnO	CaO	K_2O	Na_2O	P_2O_5	TiO_2	Total
	%										
Hematite	0.51	98.40	0.05	0.01	0.04	0.07	0.07	0.14	0.09	—	99.02
Magnetite	1.11	103.32*	0.01	0.04	0.04	0.03	0.02	0.03	0.01	0.03	104.64
Celadonite	51.35	26.37	2.68	5.56	0.03	0.10	9.73	0.16	—	0.02	96.00
Goethite (and traces of kaolinite)	3.53	81.02	0.86	0.11	0.11	0.07	0.10	0.29	0.48	0.01	86.58

* All Fe is expressed as Fe_2O_3.

5% of the volume of the parent rock consists of small grains (5 to 60 μm) of celadonite some of which were replaced by fibrous goethite associated with traces of kaolinite.

Chemical microanalyses of the different minerals of the parent rock, with the exception of quartz, are shown in Table 1. Crystallographic data of hematite and goethite are shown in Table 2.

The parent rock is intersected by veins of quartz and more rarely of dolerite. The major patterns of weathering can be outlined from bottom to top of the profile by means of microscopic, mineralogical, and geochemical characteristics as follows.

Weathering of the itabirite begins with crumbling of the quartz microlayers. Under the microscope, this involves marginal corrosion and partial separation of the quartz grains along their boundaries together with the appearance of goethite septa in the intervening spaces (Figure 3). Similar observations have been made in Australian examples (Morris 1985). Microprobe analysis showed that this goethite is aluminous-poor, but contains traces of phosphorus and titanium (Table 3) and is well crystallized (Table 2). As soon as the first stages of weathering occur, celadonite no longer exists. It is entirely pseudomorphosed by goethite associated with traces of kaolinite (Table 1). Hematite and relicts of magnetite are not yet affected. The original structure of the rock, including microfolds and veins, is perfectly preserved.

Higher in the weathering profile, quartz microlayers become hollowed whereas, remaining quartz grains are deeply corroded and seem to "float" between goethite septa (Figure 3). The dissolution of the bulk of the quartz increased the porosity although the original structure of the rock is preserved. Septa of goethite begin to develop in the intervening spaces between individual hematite crystals. The goethite gradually increases, at the expense of hematite, into spots in a centripetal manner until hematite is completely transformed. Isolated areas of magnetite within hematite remain unaltered.

In the upper part of weathering profiles, grains of hematite are separated from each other and even highly cut out into several patches, each one keeping the crystallographic orientation of the original grain, for example same extinction under crossed nichols. Goethite in septa strongly increased but does not occupy all the space left by hematite. Magnetite no longer exists. The original structure of the rock is still intact, but it is now fragile and in places, powdery. Fine tubules and millimetre size alveoles sharply intersect hematite microlayers.

At about 10 meters below the topographic surface, the profile grades the transition into a very indurated ferruginous crust of several tenths of centimetres thick (Figure 4). A brick-red, very fine-grained plastic material (called in this paper brm) fills all tubules and alveoles. Under the microscope, brm infiltrates grain

Table 2. Crystallographic characteristics of hematites and goethites of Capanema.

	aÅ	bÅ	cÅ	VÅ	MCD110Å	MCD111Å	% molAl
Hematite of Fresh Itabirite	5.036	—	13.761	302.21	424	—	0[1]
Goethite of Fresh Itabirite	4.605	9.959	3.029	138.91	477	440	0
Goethite in septa	4.611	9.939	3.029	138.81	535	367	0
Hematite after brm (patches)	5.036	—	13.79	302.90	329	—	0[1]
Goethite after brm (spots)	4.606	9.945	3.018	138.25	315	198	4
Hematite brm-head sample	5.031	—	13.764	301.65	244	—	3[2], 4.4[3]
Hematite brm-head sample	5.024	—	13.78	301.33	314	—	7[2], 9[3]
Hematite brm-fraction finer than 0.45 μm	5.025	—	13.75	300.56	219	—	6.6[2], 8[3]
Goethite brm-head sample	4.597	9.925	3.008	137.24	210	184	7
Goethite brm-head sample	4.593	9.93	3.009	137.20	262	259	8
Goethite brm-fraction finer than 0.45 μm	4.594	9.959	3.019	138.1	127	200	3

[1] After Stanjek & Schwertmann 1992.
[2] After Perinet & Lafont 1972.
[3] After Schwertmann & Kämpf 1985.

https://doi.org/10.1346/CCMN.1996.0440102 Published online by Cambridge University Press

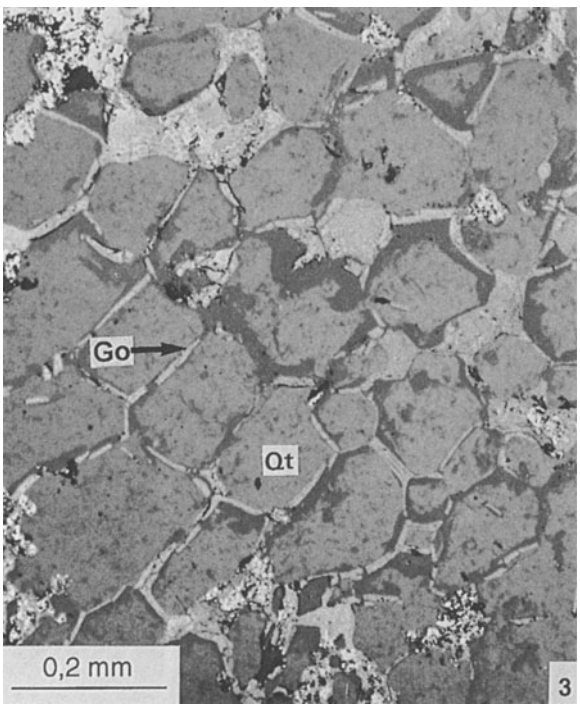

Figure 3. Goethite (Go) septa surrounding voids created by the dissolution of the quartz crystals. Reflected light.

contacts and voids and gradually develops between the different minerals forming the weathered itabirite (Figure 5). It replaces the different minerals to form ovoid, centimeter to decimeter size concentrations, elongated parallel to the topographic slope. With the naked eye, one can see these concentrations sharply cross-cutting fragile structures of the weathered itabirite without deforming them. However, no original structure is recognizable within these concentrations of brm.

Further up the profile within the highly indurated ferruginous crust (canga), the brm becomes more abundant and indurated, changing from red to violet-red, then ochre-yellow. Ferruginous nodules devoid of

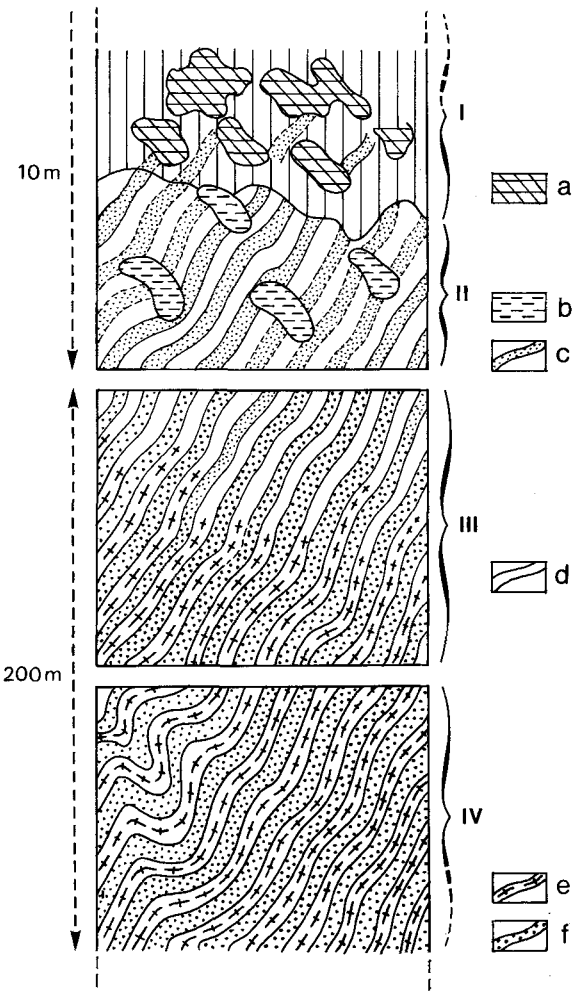

Figure 4. Sketch of evolution of the weathering profile developed on itabirites. I. Indurated ferruginous crust with coarse hematitic and goethitic nodules (a). II. Transitional horizon with disjunction of hematite + goethite septa microlayers (c) and with volumes of brick*red material (b). III. Saprolite with strongly dissolved quartz microlayers (d). IV. Parent rock with alternating microlayers of quartz (e) and of hematite + partly oxidized magnetite (f).

Table 3. Average chemical compositions of oxides and oxyhydroxides of itabirite alteration horizons--Microprobe analyses.

	SiO_2	Fe_2O_3	Al_2O_3	MgO	MnO	CaO	K_2O	Na_2O	P_2O_5	TiO_2	Total
Goethite in septas	1.33	83.30	0.20	0.11	0.08	0.03	0.02	0.04	0.06	0.01	85.18
Brick-red material (brm) a)	0.08	70.68	1.80	0.04	0.05	0.06	0.01	0.05	0.51	0.51	73.79
brm a)	0.43	70.30	4.72	0.14	0.04	0.07	0.05	0.35	0.88	0.38	77.36
brm b)	0.14	69.19	6.99	0.03	0.02	0.11	0.05	0.07	0.80	0.73	78.13
Hematite after brm (a) (patches)	0.16	89.27	2.37	0.01	0.03	0.09	0.05	0.08	0.68	0.86	93.60
Goethite after brm (b) spots	1.05	71.70	5.81	0.12	—	0.09	0.15	0.42	0.54	0.08	79.96
Goethite after brm (b) (spots)	0.20	73.12	7.38	0.02	0.03	0.02	0.06	0.08	0.54	0.20	81.65

[a] Bottom of transition.
[b] Upper part of transition (bottom of ferruginous crust).

https://doi.org/10.1346/CCMN.1996.0440102 Published online by Cambridge University Press

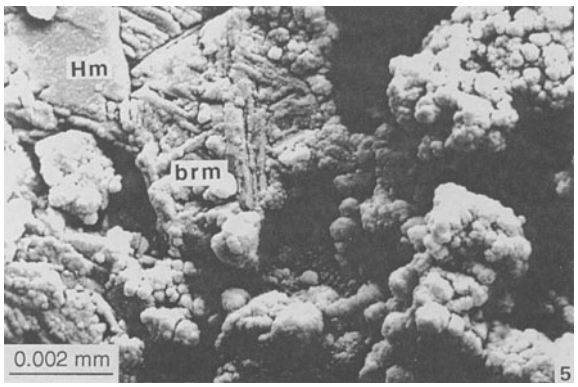

Figure 5. The brick red material (brm) replaces a hematite grain (Hm). Note the characteristic triangular patterns of hematite after magnetite (Scanning electron microscope).

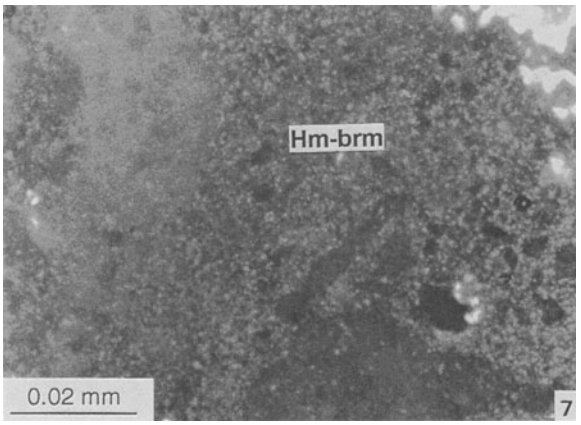

Figure 7. Hematite (Hm-brm) developing in patches within the brm. Transmitted light.

any recognizable original structure also develop. From the petrographic examination, the evolution of the brm into an indurated ferruginous facies occurs along two different paths:

1. Goethite in spots (about 8 μm of average size) develops within the brm. If desiccation cracks occur within the brm, their traces persist in the goethite but they are larger expressing a very localized volume decrease (Figure 6). This evolution continues until almost complete disappearance of the brm, which remains only as relicts within the spots of goethite.

2. Hematite, in 20 to 100 μm patches, develops within the brm. These patches coalesce, isolating remains of the brm (Figure 7). This path is often only an intermediate process at the base of the transition because hematite patches are rapidly replaced in turn by the above-mentioned goethite in spots.

Fissures crossing hematite patches and spots of goethite show along their margins very minute crystals of gibbsite. Microchemical characteristics of the brm as well as those of hematite patches and goethite spots are shown in Table 3. The crystallochemical characteristics of hematite and goethite are recorded in Table 2. This brm was the object of a detailed investigation whose major results are given below.

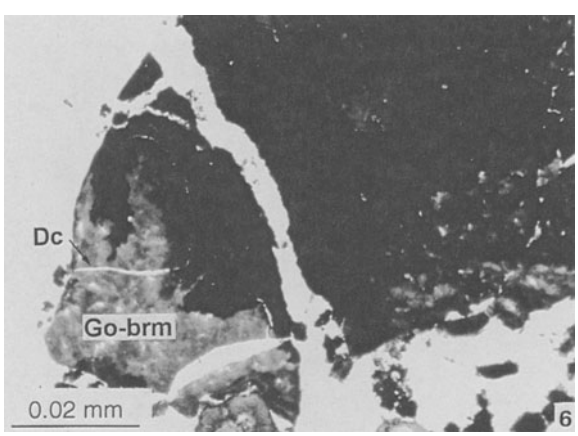

Figure 6. Goethite (Go-brm) developing within the brm. Note the desiccation cracks (Dc). Transmitted light.

THE BRICK-RED MATERIAL

Particle size analysis with a sedigraphe showed that 83 weight percent of the brm consisted of particles smaller than 0.2 μm with the remainder as large as 10 μm. Several size fractions were prepared by filtering a suspension of the brm under pressure. The head sample and two fractions (0.8–0.45 μm, and <0.45 μm) were investigated in detail.

Chemical Analyses

Chemical analyses by AAS (Table 4) are consistent with the 110 microprobe analyses (Table 3) of the brm from the top of the transition horizon. It indicates that this essentially ferruginous brm is increasingly alumina enriched within the ferruginous crust. This brm is very hydrated and contains small amounts of titanium and organic carbon.

Analyses by Chemical Extractions

No dissolution of <0.45 μm fraction of the brm occured during either oxalate at pH3 or citrate bicarbonate dithionite (CBD). This indicates the absence of amorphous or poorly-crystallized material such as ferrihydrite.

Table 4. Average chemical composition of brick-red material AAS analyses.

SiO_2	Fe_2O_3	Al_2O_3	MnO	TiO_2	H_2O^+	% org-CO_2	Total
0.40	75.70	7.50	0.03	0.47	14.80	1.23	100.20

https://doi.org/10.1346/CCMN.1996.0440102 Published online by Cambridge University Press

X-ray Diffraction Analyses

The brm approximately consists of 75% goethite and 25% hematite. Crystallographic parameters for hematite and goethite of the head sample and the <0.45 μm fraction are given in Table 2. The mean crystal dimension (MCD) of hematite is generally higher than those of associated goethite while calculated substitution rates range between 3 and 9% moles Al_2O_3 for hematite and between 3 and 8% moles AlOOH for goethite.

Analyses by Mössbauer Spectrometry

Five samples were studied by Mössbauer spectrometry: primary hematite (from fresh itabirite), goethite from septa, and three different size fractions of the brm (head sample, 0.8–0.45 μm fraction, and <0.45 μm fraction). Mössbauer spectra were recorded at 298°K for the five samples and a spectrum at 77°K was also recorded for the brm finest fraction.

PRIMARY HEMATITE. The 298°K Mössbauer spectrum of the primary hematite can be well fitted with only one sextet (Figure 8-1 and Table 5). The value of the hyperfine field (51.8 T) matches that for well-crystallized pure hematite (Fysh and Clark 1982; Murad and Schwertmann 1986). This indicates that the mineral does not contain detectable amounts of Al. Janot et al. (1973) made use of the lowered magnetic ordering temperatures to set up particle size groups for superparamagnetic Fe-oxides. The lack of a superparamagnetic component in the Mössbauer spectrum at 298°K of the primary hematite is indicative of a mean crystal dimension (MCD) greater than 400 Å. This result is in good agreement with XRD data.

GOETHITE FROM SEPTA. The Mössbauer spectrum at 298°K of this goethite shows resonant lines with a lower asymetrical broadening and a magnetic hyperfine field of about 37.8 T (Table 5). According to Murad (1982) these data characterize a goethite with good crystallinity, MCD above 300 Å and without Al-substitution.

THE BRICK-RED MATERIAL. All Mössbauer spectra of the brm recorded at 298°K include both magnetic and paramagnetic contributions (Figure 8-2 to 8-4). Spectra were fitted using sextets for the magnetic part. The superparamagnetic part of the spectra was fitted by a sum of a doublet and three sextets with decreasing and low internal magnetic fields, and high line width. Similar approaches were previously used in order to fit Mössbauer spectra with paramagnetic relaxation (Fysh et al. 1983a and b; Murad and Wagner 1991). For the three size fractions of brm (Figure 8-2, 8-3, and 8-4), the Mössbauer parameters of the lines corresponding to the paramagnetic function are quite the same, showing that this approach presents an internal consistency. In the spectrum of the brm head sample (Table 5, Figure 6-2), sextets 1 and 2 have Mössbauer parameters very close to those of the primary hematite and the goethite from septa. The paramagnetic phase contains about 70% of iron atoms. In the finer fractions of the brm sample (Figure 8-4), only a sextet with an internal magnetic field near 50.3 T is present and can be attributed to an hematite phase, while the sextet corresponding to the goethite phase is absent. The hematite sextet has a low internal magnetic field and broad line widths. The first feature suggests an hematite phase slightly Al-substituted and/or having a low crystallinity. The line broadening suggests a nonhomogeneous phase with a distribution of Mössbauer parameters. As the particle size of brm decreases, the amount of the paramagnetic phase increases from about 70 to 85%.

A Mössbauer spectrum of the finest fraction (particles <0.45 μm) was also recorded at 77°K, because it is in this fraction size that amorphous or very poorly-crystallized iron oxides, like ferrihydrite, can occur. The experimental spectrum (Figure 8-5) shows only magnetic contributions and can be well fitted using three sextets. According to Murad and Schwertmann (1986), the sextet with a high hyperfine field at 77°K (52.8 T) could be attributed to an hematite phase in the weak ferromagnetic (wfm) state (Murad 1987) with low Al-substitution and similar to the primary hematite. The sextet with the lower internal magnetic field (47.0 T) can be unambiguously attributed to goethite (Murad 1982). Because the measured internal magnetic field is lower than that determined for crystallized and Al-free goethite (Murad 1987), this goethite is Al-substituted and/or has a low crystallinity. Golden et al. (1979) gave a dependence law of the magnetic field of goethite at 77°K related to Al-substitution and crystallinity. Though the study was criticized by Fysh and Clark (1982), it is used here qualitatively as follows.

If, as a first approach, the effect of crystallinity is neglected, then using the relation given by Golden et al. (1979) the Al-substitution rate found for this goethite is near 20%. Alternatively, if the reduction of the magnetic field is only related to a crystallinity effect, the mean MCD values for this goethite could be expected to be in the range of 80 to 150 Å (Janot et al. 1973). From XRD data, goethite in this size fraction of the brm has MCD values in the range of 130 to 200 Å, and the Al by Fe substitution rate is near 3 mole %. Therefore according to both Mössbauer and XRD data, this goethite phase has relatively low crystallinity (MCD below 200 Å) and moderate Al substitution.

The hyperfine field of the last sextet is 49.4 T. This is the value classically observed for goethite (at 77°K) in the case of absence of particle size effects and Al-substitution (Murad 1987). Because an equivalent component is not observed in the 298°K Mössbauer spectrum of this sample, this last sextet cannot be attributed to goethite. According to XRD data, this size

https://doi.org/10.1346/CCMN.1996.0440102 Published online by Cambridge University Press

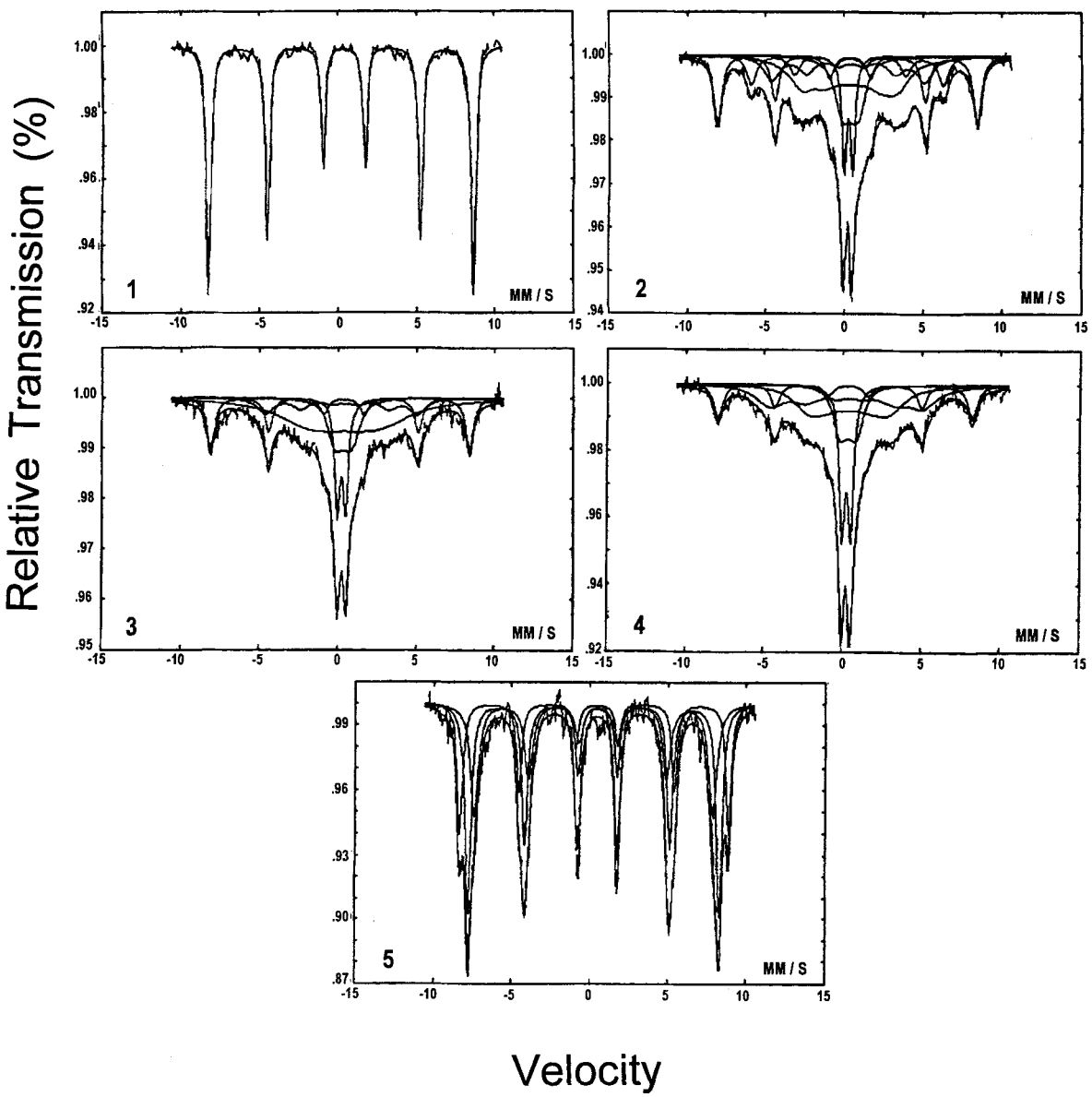

Figure 8. Mössbauer spectra of: 1. hematite from fresh itabirite (298°K). 2. brm, head material (298°K). 3. brm, 0.45–0.8 μ fraction (298°K). 4. brm, less than 0.45 μm fraction (298°K). 5. brm, less than 0.45 μm fraction (77°K). Broken line = experimental; continuous lines = fit.

fraction of brm contains an Al-substituted hematite phase, having a low crystallinity. The mineralogical complexity of the sample (mixing of two hematite phases) limits more precise conclusions.

In summary, the Mössbauer data indicate that the brm does not contain amorphous iron phase or ferrihydrite and that the main components are of two kinds:

1) inherited hematite and goethite, the latter being more abundant in the coarser fractions and absent in the <0.45 μm fraction; and

2) new hematite and goethite phases, both characterized by Fe with Al substitutions and small MCD values. In the <0.45 μm fraction (which represents more than 85% of the brm) the authigenic Al-goethite contains 34% and the authigenic Al-hematite 42% of iron atoms within the sample (Table 5).

DISCUSSION AND CONCLUSIONS

Most of the thick weathering profile (~ 200 meters) developed on the itabirites of Capanema is characterized by:

1) Gradual and almost total loss of quartz.

https://doi.org/10.1346/CCMN.1996.0440102 Published online by Cambridge University Press

Table 5. Mössbauer parameters of studied samples.

Sample	Temperature (K)	Mössbauer line	H Tesla	Q.S. mm/s	I.S. mm/s	Γ mm/s	Relative area (%)
Hematite of fresh itabirite	298	Sex.	51.8	−0.17	0.35	0.34	100
Goethite from septa	298	Sex.	37.8	−0.38	0.35	0.40	100
Brick-red material:	298	Sex. 1	50.8	−0.19	0.33	0.60	21
(head sample)		Sex. 2	37.8	−0.2	0.34	0.70	11
		Sex. 3	31	−0.2	0.34	1.00	15
		Sex. 4	19	−0.2	0.34	2.00	27
		Sex. 5	4	−0.2	0.34	1.00	16
		Doublet	—	0.55	0.34	0.35	10
Brick-red material:	298	Sex. 1	50.3	−0.19	0.34	0.60	20
(0.45 to 0.8 μm		Sex. 2	31.2	−0.23	0.34	1.25	13
fraction)		Sex. 3	17.0	0	0.34	2.50	37
		Sex. 4	4.3	0	0.39	1.00	16
		Doublet	—	0.55	0.34	0.41	14
Brick-red material:	298	Sex. 1	50.3	−0.215	0.35	0.70	15
fraction finer		Sex. 2	31.2	−0.2	0.35	2.20	26
than 0.45 μm		Sex. 3	17	0	0.35	2.10	25
		Sex. 4	4.3	0	0.36	0.90	15
		Doublet	—	0.56	0.35	0.43	19
	77	Sex. 1	49.4	−0.24	0.45	0.40	42
		Sex. 2	52.8	−0.17	0.45	0.38	24
		Sex. 3	47.0	−0.24	0.46	0.60	34

Sex. = Sextet; H = internal magnetic field; Q.S. = Quadrupole Splitting; I.S. = isomer shift (v.s. Fe metal): Γ = half maximum line width.

2) Appearance of goethite in septa, which in the previous microlayers of quartz plays the role of pillars maintaining the original structures without collapse of dissolved beds.
3) Disjunction of primary hematite and its very localized replacement by goethite within the septa.

Macroscopic and microscopic data indicate that the original structures of the parent rock, that is the original volume, were preserved during weathering. Ramanaïdou (1989, p.111) clearly showed that most of the observed voids had a size essentially identical to that of the remaining fresh quartz grains and that dissolved quartz corresponded very closely to the porosity percentage. As a whole, the disjunction of primary hematite is compensated by precipitation of goethite within the septa. All these data fully justify the isovolume reasoning of Millot and Bonifas (1955) for the calculation of geochemical budgets. This weathering profile with preserved structure is a saprolite (Figure 4). In the upper part of the saprolite over a thickness of several centimeters to a few meters, the transition to the indurated ferruginous crust occurs. This crust (canga) is about 10 meters thick and comprises coarse nodules in which the original structure is erased. In this transition horizon (Figure 4), the brm plays a fundamental role in the genesis of the ferruginous duricrust. The brm develops within the upper part of the powdery saprolite and replaces primary hematite and goethite in the septa. This replacement is gradual and occurs without apparent deformation of the fragile structures of the powdery saprolite. Therefore, this replacement is pseudomorphic and occurs at constant volume. This situation recalls previous observations of ferruginous concentrations in laterites of tropical Africa (Nahon 1976, 1991) whose physico-chemical mechanisms and limitations were recently established (Merino et al. 1993). Isovolumetric geochemical budgets with respect to the powdery saprolite in which the brm develops indicates loss of iron (−45% Fe_2O_3) but increase in alumina (+84% Al_2O_3) (Tables 1, 3, 4 and 6).

Table 6. Specific gravity and porosity of the brm, the saprolite, and the nodules.

	Specific gravity	Porosity (%)
brm	1.7	59
Indurated nodules	2.9	39
Powdery saprolite	2.5	45

The brm is a highly hydrated material and is today a functional medium in which previous hematite and goethite appear unstable. They are progressively replaced by Al substituted new goethite (predominant) and hematite phases. The brm contains detectable amounts of organic carbon. Downward percolating solutions through the upper ten meters of the profile contained organic complexants that could play a role in the transfer of iron and aluminum. As noted previously by Kampf and Schwertmann (1982), organics favor the hematite-goethite transformation. Nevertheless in the present study, the occurrence of organic matter has

no inhibitory effect on the crystallization of iron oxides (Schwertmann 1966). No amorphous hydrous ferric oxide and/or ferrihydrite are observed.

The appearance of new Al substituted goethite and hematite phases in the brm suggests that aluminum activity of solutions, in the upper part of the profile, appears as the motor of the geochemical system. Numerous papers dealing with the influence of aluminum on the formation of iron oxides were published from experimental data, thermodynamic approach, and natural observations, leading to conflicting results on the favored phase (Lewis and Schwertmann 1979; Tardy and Nahon 1985; Schwertmann and Kämpf 1985; and a review in Schwertmann 1988b).

The origin of the discrepancy between the different approaches is probably, as discussed by Schwertmann (1988b), due to the role of other parameters that influence the chemical reactions such as water activity, pH, and temperature, etc. In the present study, Al substituted goethite and hematite appears simultaneously, but with a dominant goethite phase.

The rate of dissolution-precipitation of minerals can also play a great role in the hematite/goethite ratio observed in weathering profiles. Within the brm, relictual goethite from septa are absent in finer fractions and is preserved only in the coarser fractions, while relictual hematite survives in all fractions. This indicates a greater weatherability of relict goethite versus relict hematite.

The process of hematite and goethite formation in the FeIII system has been often discussed (Schwertmann 1988b). If goethite forms directly from solution, possibly after dissolution of a precursor phase like ferrihydrite, hematite seems to form within ferrihydrite aggregates. Recently Combes et al. (1990) detailed the mechanisms by which freshly precipitated hydrous gel transformed into hematite through a transient phase similar to ferrihydrite. In the brm where hematite grows, no detectable amounts of amorphous iron oxides or ferrihydrite were detected. So if a ferrihydrite-like phase is a necessary precursor of hematite, its transient character should be extremely pronounced in lateritic profiles because similar observations were often noticed in studies of tropical weathering (Nahon et al. 1977; Ambrosi and Nahon 1986). In the work of Combes et al. (1990), the transient phase disappeared completely after aging during 130 h at 92°C of anhydrous gel. The high rate of transformation of the precursor into hematite can explain the lack of observation of such a phase in lateritic weathering profiles. Ferrihydrite should be more often described in soil profiles developed under temperate climates where low-rate reactions are favored. Another interpretation can be the direct formation of hematite from the solution without a precursor. The present data are consistent with such a mechanism.

Macroscopic and microscopic observations show that the brm evolves toward ferruginous nodules, which form most of the indurated ferruginous crust. The brm is less aluminous at the base of the transition horizon than at the top. This is true for goethite and hematite replacing the brm during induration in the form of nodules.

All the previous data indicate an evolution of the brm into indurated ferruginous nodules in which no structure of the saprolite subsists. Furthermore, average geochemical budgets between brm and indurated nodules, calculated from Tables 3 and 6 by the isovolumetric method (Millot and Bonifas 1955) show aluminum maintained and Fe_2O_3 increased by 40% in indurated nodules.

If indurated nodules are mainly hematitic at the top of the transition horizon, aluminous goethite becomes rapidly predominant starting from the bottom of the indurated ferruginous crust (canga). Consequently, goethitization becomes generalized at the top of the weathering of itabirites. A question remains, the source of aluminum. It may be assumed that the deeply-weathered dolerite veins in the upper part of the profile can provide this aluminum. The Al-Ti geochemical signature of the brick-red material and of the aluminous hematite and goethite of the top of the profile seems to support this assumption.

ACKNOWLEDGMENTS

We thank the CNRS (INSU) for financial support and grant MRT 90LO712, Universidade de São Paulo (Brazil) for supporting D. Nahon and E. Ramanaïdou. Thanks to B. Boulangé, R. Dassulle, J.-J. Motte, N. Pelegrin from University Aix-Marseille 3, J -J. Trescases from University of Poitiers, for their help and to A. V. Carozzi (University of Illinois), R. C. Morris (CISRO, Perth) for their helpful discussions and their English corrections. We thank R. E. Ferrell Jr. as editor in chief, R. Gilkes and an anonymous reviewer for their constructive suggestions.

REFERENCES

Ambrosi JP, Nahon D. 1986. Petrological and chemical differentiation of lateritic iron crusts profiles. Chem Geol 57: 371–393.

Combes JM, Manceau A, Calas G. 1990. Formation of ferric oxides from aqueous solutions: a polyhedral approach by X-Ray spectroscopy; II. Hematite formation from ferric gels. Geochem Cosmoch Acta 54:1083–1091.

de Campos EN. 1980. Etude de l'altération en pays tropical humide d'une formation précambrienne à itabirites et roches volcaniques. Serra do Carajas, Amazonie, Brésil. Thèse Univ. Strasbourg, unpubl. 300 p.

Dorr JVN II. 1969. Physiographic, stratigraphic and structural development of the Quadrilatero Ferrifero, Minas Gerais, Brazil. USGS Prof. Paper, 641A. 110 p.

Eichler J. 1968. O enrequecimento residual e supergenico dos itabiritos atraves do intemperismo. Geologia I:29–40.

Fysh SA, Clark PE. 1982. Aluminous hematite: a Mössbauer study. Phy Chem Miner 8:257–267.

Fysh SA, Cashion JD, Clark PE. 1983a. Mössbauer effect studies of iron in kaolin. J. Structural iron. Clays & Clay Miner 31:285–292.

Fysh SA, Cashion JD, Clark PE. 1983b. Mössbauer effect

studies of iron in kaolin II Surface iron. Clays & Clay Miner 31:293–298.
Golden DC, Bowen LH, Weed SB, Bigham JM. 1979. Mössbauer studies of synthetic and soil-occuring aluminium substituted goethites. Soil Sci Soc Am J 43:802–808.
Janot C, Gibert H, Tobias C. 1973. Caractérisation des kaolinites ferrifères par spectrométrie Mössbauer. Bull Soc Fr Mineral Cristallogr 96:281–291.
Kampf N, Schwertmann U. 1982. Goethite and hematite in a climosequence in Southern Brazil and their application in classification of kaolinite soils. Geoderma 29:27–39.
Klug HP, Alexander LE. 1962. X-Ray Diffraction Procedures. New York: John Wiley and Sons, Inc.
Klug HP, Alexander LE. 1974. X-Ray Diffraction Procedures for Polycrystalline and Amorphous Materials. New York: J. Wiley and Sons. 966 p.
Lewis DG, Schwertmann U. 1979. The influence of aluminium on the formation of iron oxides. IV. The influence of [Al], [OH], and temperature. Clays & Clay Miner 27:195–200.
Melfi AJ, Pedro G, Nalovic L, Queiroz Netto JP. 1976. Etude sur l'altération géochimique des itabirites du Brésil. Cah. ORSTOM, Sér. Pédologie, XIV 3:179–192.
Merino E, Nahon D, Wang Y. 1993. Kinetics and mass transfer of pseudomorphic replacement: application to replacement of parent minerals and kaolinite by Al, Fe and Mn oxides during weathering. Am J Sci 293:135–155.
Millot G, Bonifas M. 1955. Transformations isovolumétriques dans les phénomènes de latéritisation et de bauxitisation. Bull Serv Carte Géol Alsace-Lorraine 8:3–10.
Morris RC. 1983. Supergene alteration of banded iron formation. In:Trendall AF, Norris RC, editors. Iron Formations: Facts and Problems. Amsterdam:Elsevier. 513–534.
Morris RC. 1985. Genesis of iron ore in banded iron-formation by supergene and supergene-metamorphic processes. A conceptual model. In:Wolf K.H., editor. Handbook of Strata-Bound and Stratiform Ore Deposits. Amsterdam:Elsevier. 13:73–235.
Murad E. 1982. The characterization of goethite by Mössbauer spectroscopy. Am Miner 67:1007–1011.
Murad E, Schwertmann U. 1986. The influence of Al-substitution and crystallinity on room temperature Mössbauer spectrum of hematite. Clays & Clay Miner 34:1–6.
Murad E. 1987. Properties and behavior of iron oxides as determined by Mössbauer spectroscopy. In:Stucki JW, Goodman BA, Schwertmann U., eds. Iron in soils and Clay Minerals. Dordrecht: D. Reidel. 309–350.
Murad E, Wagner U. 1991. Mössbauer spectra of kaolinite, halloysite and the firing products of kaolinite: new results and a reappraisal of published work. Neues Jahrburh Miner Abh 162:281–309.
Nahon D. 1970. Nouvelles observations sur les faciès d'altérations anciennes au Sénégal et en Mauritanie. Travaux des Laboratoires des Sciences de la Terre, St-Jérôme Marseille, série A 2. 50 p.
Nahon D. 1976. Cuirasses ferrugineuses et encroûtements calcaires au Sénégal occidental et en Mauritanie. Systèmes évolutifs: géochimie, structures relais et coexistence. Strasbourg: Mém Sci Géol 44:229 p.
Nahon D, Janot C, Karpoff AM, Paquet H, Tardy Y. 1977. Mineralogy, petrography and structures of iron crusts developed on sandstones in the western part of Senegal. Geoderma 19:263–277.
Nahon D. 1991. Introduction to the petrology of soils and chemical weathering. New York:Wiley and Sons. 313p.
Perinet G, Lafont R. 1972. Sur les paramètres cristallographiques des hématites alumineuses. CR Acad Sci Paris C 275:1021–1024.
Ramanaidou E. 1989. Evolution supergène des itabirites protérozoïques de la mine de fer de Capanema, Minas Gerais, Brésil. Thèse Univ. Poitiers, unpublished, 183 p.
Rassineux F, Beaufort D, Merceron T, Bouchet A, Meunier A. 1988. Use of localization detector for XRD of very small quantities of matter. Clays & Clay Minerals 36:187–189.
Schulze DG. 1982. The identification of iron oxides by differential XRay Diffraction and the influence of aluminium substitution on the structure of goethite. Ph. D. thesis, Univ. Munich, unpublished.
Schwertmann U. 1966. Inhibitory effect of soil organic matter on the crystallization of amorphous ferric oxide. Nature 212:5062, 645–646.
Schwertmann U. 1986. The effect of pedogenetic environments on iron oxide minerals. Adv Soil Sci I:171–200.
Schwertmann U. 1988a. Some properties of soil and synthetic iron oxides. In: Stucki JW, Goodman BA, Schwertmann U, editors. Iron in soils and clay minerals. Dordrecht, Reidel. 203–250.
Schwertmann U. 1988b. Occurence and formation of iron oxides in various pedoenvironments. In: Iron in soils and clay minerals. Stucki JW, Goodman BA, Schwertmann U, editors. Dordrecht, Reidel. 267–308.
Schwertmann U, Kampf N. 1985. Properties of goethite and hematite in kaolinite soils of southern and central Brazil. Soil Sci 39:344–349.
Stanjek H, Schwertmann U. 1992. The influence of aluminium on iron oxides. Part XVI: hydroxyl and aluminium substitution in synthetic hematites. Clays & Clay Miner 40: 347–354.
Tardy Y, Nahon D. 1985. Geochemistry of laterites, stability of Al-goethite, Al-hematite and Fe^{3+} kaolinite in bauxites and ferricretes. Am J Sci 285:865–903.
Tournarie M. 1969. Evaluation optionale des inconnues d'un système étatique non linéaire. I. Principe et Théorie. J Phys 30:737–751.

(Received 29 June 1994; accepted March 1995; Ms. 2530)